A&A 395, 955–967 (2002)
DOI: 10.1051/0004-6361:20021304


Astronomy & Astrophysics

# An HI interstellar bubble linked to the O-type stars BD +24°3866 and BD +25°3952

C. Cappa[1,2,⋆], S. Pineault[3], E. M. Arnal[1,2,⋆], and S. Cichowolski[1,⋆⋆]

[1] Instituto Argentino de Radioastronomía, C.C. 5, 1894 Villa Elisa, Argentina
[2] Facultad de Ciencias Astronómicas y Geofísicas, Universidad Nacional de La Plata, Paseo del Bosque s/n, 1900 La Plata, Argentina
[3] Département de Physique et Observatoire du Mont Mégantic, Université Laval, Québec, Canada G1K 784

Received 12 April 2002 / Accepted 5 September 2002

**Abstract.** We investigate the ISM in the vicinity of the O-type stars BD +24°3866 (O8.5II(f)), BD +24°3881 (O6.5III(f)) and BD +24°3952 (O8) based on radio continuum and HI line data obtained with the Synthesis Telescope of the Dominion Radio Astrophysical Observatory (DRAO) with synthesized beams of 1.′5 and 7′ at 1420 and 408 MHz, respectively. High angular resolution *IRAS* data (*HIRES*) are also analyzed. BD +24°3866 is found to be located close to the inner border of a slowly expanding shell. The evolved HII region Sh2-88, which is excited by BD +25°3952, appears to be interacting with neutral material in the approaching part of this shell. The whole structure is at a distance of 2.4 kpc and is about 23×15 pc in radius. The total swept up mass is 1300 $M_{\odot}$. The stellar winds of BD +24°3866 and BD +25°3952, are mainly responsible for shaping the HI structure. An HI expanding shell was also found to be related to the HII region G61.7+0.9. At a kinematic distance of 2.4 kpc, this feature is 10 pc in radius and has neutral and ionized masses of 200 and 135 $M_{\odot}$, respectively. The present observational data do not allow us to identify a definite interstellar HI feature associated with BD +24°3881. We consider different explanations for this fact.

**Key words.** ISM: bubbles – HII regions – ISM: individual objects: Sh2-88, Sh2-87, G61.7+0.9 – stars: early-type – stars: individual: BD +24°3866, BD +24°3881, BD +25°3952

## 1. Introduction

It is well established that the structure and kinematics of the interstellar medium (ISM) are strongly affected by the action of stellar winds from massive stars. With mass loss rates spanning the interval $10^{-7} \leq \dot{M} \leq 10^{-5}\ M_{\odot}\ \mathrm{yr}^{-1}$ (e.g. Chlebowski & Garmany 1991) and terminal velocities $V_{\mathrm{w}}$ in the range 1000–3000 km s$^{-1}$ (Prinja et al. 1990), stellar winds from early-type stars create hot ($T = 10^6$–$10^7$ K) and very rarefied ($n_{\mathrm{e}} \simeq 0.01$ cm$^{-3}$) regions bounded by an outer expanding envelope. This region, known as an *interstellar bubble*, has a complex structure (Weaver et al. 1977; Koo & McKee 1992).

From the observational point of view, bubbles around Wolf-Rayet (WR) and Of stars were searched for by several authors (e.g. Lozinskaya 1982; Chu et al. 1983; Miranda & Rosado 1987; Marston et al. 1994) from H$\alpha$ images and Fabry-Perot data. In the radio wavelength regime, both ionized and neutral expanding shells have been found associated with both WR and O-type stars (see Cappa et al. 1996; Cappa & Herbstmeier 2000; Cichowolski et al. 2001 and references therein). In the case of interstellar bubbles observed around WR stars, their large dimensions together with their low expansion velocities suggest that the massive progenitor (an O-type star) of the current WR star must also be responsible for shaping the bubbles. Consequently, O- and Of-type stars are promising candidates to investigate the effects of stellar winds on the surrounding gas. Although several HI voids and shells around massive stars have been analyzed mainly based on data gathered with instruments having low and intermediate angular resolution, high angular resolution observations are crucial to help understanding the ISM-stellar wind interaction.

Based on HI line and radio continuum observations at 1420 and 408 MHz obtained with the Synthesis Telescope of the Dominion Radio Astrophysical Observatory (DRAO), we analyze the interstellar medium local to the Of stars BD +24°3866 and BD +24°3881. Complementary radio, infrared and molecular data are also examined.

## 2. Observational data

### 2.1. Radio data

The field of the O-type stars was observed at 408 MHz (continuum) and 1420 MHz (continuum and HI line) using the Synthesis Telescope of the DRAO in April 2000. The DRAO

*Send offprint requests to*: C. Cappa,
e-mail: ccappa@fcaglp.fcaglp.unlp.edu.ar
⋆ Member of CONICET, Argentina.
⋆⋆ Fellowship of CONICET, Argentina.

Synthesis Telescope is an array of seven antennas, aligned on an *EW* baseline. An updated description of the telescope can be found in Landecker et al. (2000). The telescope produces wide-field, high quality images with a synthesised beam of about 1′ at 21 cm. Full synthesis was performed. The relevant instrumental parameters are summarized in Table 1.

The continuum and HI data were calibrated and transformed into sky images by the DRAO staff following standard procedures. The subsequent data reduction was performed using DRAO software. Regarding the HI data, the out-of-band continuum was subtracted from the channel maps. The images were cleaned and self-calibrated.

Flux correction factors were then applied at 408 MHz using sources from the Texas 365-MHz Survey (Douglas et al. 1996) and the 4C Survey (Pilkingston & Scott 1965) and at 1420 MHz based on the NRAO/VLA Sky Survey (NVSS, Condon et al. 1998). Uncertainties in calibration are about 15% and 10% at 408 and 1420 MHz, respectively.

The missing short-spacing information for the continuum images was obtained from the Effelsberg 21 cm Galactic Plane Survey (Kallas & Reich 1980) and from the 408 MHz All-Sky Survey (Haslam et al. 1982). With regard to the HI line data, a square region, 4° in size, was observed using the 26m DRAO telescope. These observations were carried out using bandwidth specifications that exactly matched those used while collecting the interferometric line data. Single dish data were calibrated in brightness temperature against the standard region S7 (Williams 1973). These data were used to fill in the missing short-spacing information in the interferometric database.

In order to increase the $S/N$ ratio, the final HI maps were spatially convolved to an angular resolution of 2.′5 using a Gaussian beam.

### 2.2. Infrared data

To investigate the dust distribution in the region, high-resolution (HIRES)[1] data in the four *IRAS* bands were also obtained with angular resolutions in the range 0.′5 to about 2′ as the result of 20 iterations of the algorithm.

## 3. Stars and HII regions in the area

BD +24°3866 (HDE 338926) and BD +24°3881 (HDE 338931) are classified as O8.5II(f) and O6.5III(f), respectively (Garmany & Vacca 1991). Along with BD +25°3952, they are considered to be members of the Vul OB1 association (Garmany & Stencel 1992) at a distance $d$ = 2.5 kpc. Table 2 lists their coordinates, spectral classification, proper motions as obtained from the Tycho-2 Catalog (Hog et al. 2000) and LSR radial velocities. Heliocentric velocities were obtained from the compilation by Barbier-Brossat & Figon (2000). These stars are the only O-type stars members of Vul OB1 projected onto the field.

[1] *IPAC* is funded by NASA as part of the *IRAS* extended mission under contract to Jet Propulsion Laboratory (JPL) and California Institute of Technology (Caltech).

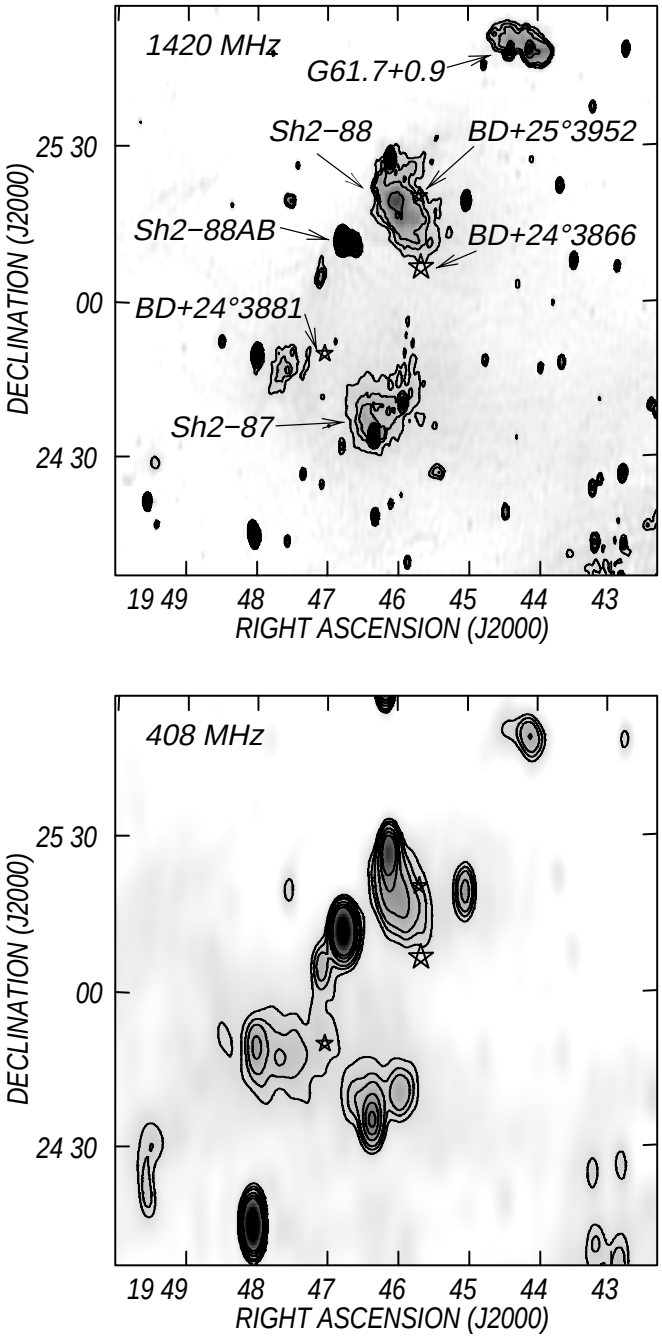


**Fig. 1.** Radio continuum observations at 1420 and 408 MHz. The star symbols mark the position of the three O-type stars in the area. The HII regions and the stars are identified in the image at 1420 MHz. Contour levels at 1420 MHz are 9.0, 9.5, 10.0, 12.0 and 14 K and 100.0 to 130.0 K in steps of 10 K at 408 MHz.

The well known HII regions Sh2-87 and Sh2-88 are present within the field (Sharpless 1959).

Sh2-87 is a faint nebulosity of about 10′ in size located at RA, Dec (J2000) = $19^{\rm h}46\overset{\rm m}{.}4$, +24°34.′3. Observations carried out with the Westerbork Synthesis Radio Telescope (WSRT) at 5 GHz resolve this region in two bright components, classified as ultracompact (UC) HII regions, having electron densities of 900 and 1400 cm$^{-3}$, respectively (Felli & Harten 1981). Georgelin (1975) suggested that the nebula might be excited by

**Table 1.** DRAO synthesis observations: relevant parameters.

| | | |
|---|---|---|
| Field center | RA (J2000) | $19^h46^m30^s$ |
| | Dec (J2000) | 24°58′ |
| | *(l,b)* | 61.°23, +0.°03 |
| Primary beams | 408 MHz | 5.°3 to 50% |
| | 1420 MHz | 1.°7 to 50% |
| Synthesized beams | 408 MHz | 2.′8 × 7.′7 |
| | 1420 MHz | 0.′8 × 2.′0 |
| Spectrometer | number of channels | 256 |
| | velocity coverage | (–190, +230) km s$^{-1}$ |
| | channel spacing | 1.6 km s$^{-1}$ |
| | velocity resolution | 2.6 km s$^{-1}$ |
| rms noise level | 408 MHz | 1.7 K |
| | 1420 MHz | 0.1 K |
| | channel maps | 2.7 K |

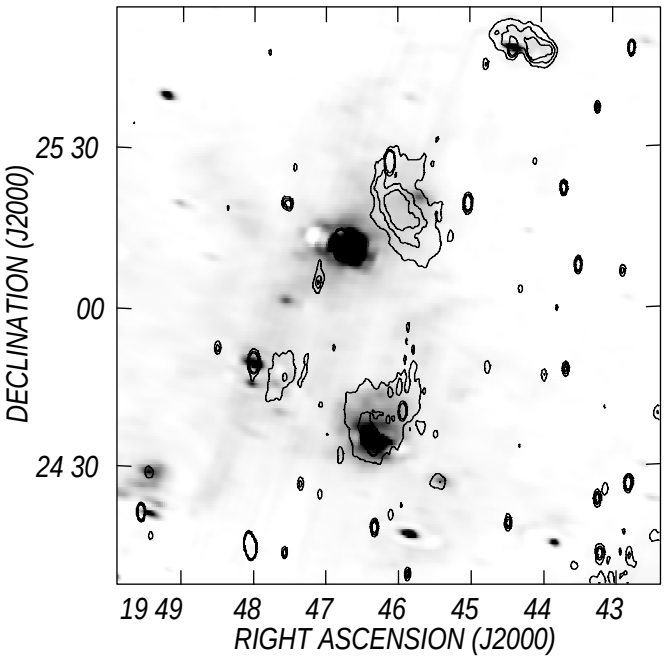


**Fig. 2.** Overlay of the HIRES 60 $\mu$m infrared *(grayscale)* and the radio continuum image at 1420 MHz *(contour lines)*. The grey scale is 1 to 300 MJy/sr. Contour lines are 9.0, 10.0 and 11.0 K.

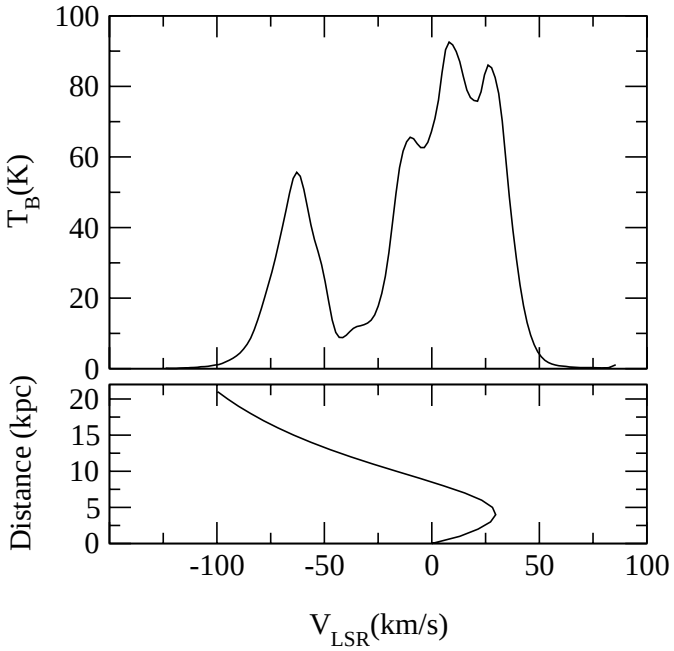


**Fig. 3.** *Top*, average HI profile within a region of 50′ in radius centered at RA, Dec (J2000) = $19^h46^m30^s$, +24°58′ [*(l,b)* = (61.°23, +0.°03)]. *Bottom*, kinematic distances toward $l = 61°$ obtained from an analytical fit to the rotation curve (Brand & Blitz 1993).

the B0.5V star HDE 338936. However, Felli & Harten claimed that this star could not provide the required Lyman-continuum photon flux and concluded that the main source of ionization is an early-type star embedded in one of the UC HII regions. Molecular material at LSR radial velocities in the range 22–24 km s$^{-1}$ has been found to be associated with the HII region (Pirigov et al. 1995). These velocities are in agreement, within errors, with the radial velocity derived from the H$\alpha$ line (19.6 km s$^{-1}$, Georgelin 1975).

As for the diffuse nebula Sh2-88 its size is about 25′ and is located at RA, Dec (J2000) = $19^h46^m$, +25°20′. Georgelin et al. (1973) and Fich et al. (1990) found H$\alpha$ LSR velocities of 25.2 and 19.8 km s$^{-1}$, respectively. Its exciting star is the O8 star BD +25°3952 (≡ HDE 338916 = LSII+25°08) (Lortet-Zuckerman 1974). Two nebular knots, named Sh2-88A and Sh2-88B of about 1′ in size each, are found toward the southeast about 15′ far from Sh2-88 (Lortet-Zuckermann 1974). The exciting star of Sh2-88A is LSII+25°9 (Lortet-Zuckerman 1974). Sh2-88B consists of a cometary HII region (B1) and a UC HII region (B2) and coincides with both the radio source G61.48+0.09 and the infrared source IRAS 19446+2505 (see Deharveng et al. 2000 for a description of Sh2-88B). OH emission related to Sh2-88 was found at an LSR velocity of 21.8 km s$^{-1}$ by Turner (1970). Carbon monoxide and other molecular species observations toward Sh2-88 and Sh2-88B reveal molecular gas with velocities in the range 21–25 km s$^{-1}$ (e.g. Blair et al. 1975; Churchwell et al. 1990; White & Fridlung 1992; Helfer & Blitz 1997).

Distance determinations for Sh2-87, Sh2-88 and their exciting stars range from 1.7 to 2.6 kpc (e.g. Fich & Blitz 1984; Forbes 1989; Barsony 1989; Deharveng et al. 2000). In agreement with these last authors, we adopted $d$ = 2.4 kpc for the HII regions.

Both Sh2-87 and Sh2-88B are regions of active star formation as indicated by the presence of $H_2O$ maser line emissions and bipolar outflows (e.g. Barsony 1989; Deharveng et al. 2000).

The radio source G61.7+0.9 is projected onto the NE part of the field. Its spectrum suggests a thermal source (Reich et al. 1986). Bronfman et al. (1996) found CS emission at –73 km s$^{-1}$ toward IRAS 19423+2541, seen projected onto the HII region. They proposed this source to be an OB star formation site.

The large scale HI distribution in the environs of Sh2-87 and Sh2-88 was previously analyzed using HI spectra taken with the Effelsberg radiotelescope ($HPBW = 9'$) by Ehlerová et al. (2001). These authors found that Sh2-87 lies inside an HI hole detected along the velocity interval +20 to +26 km s$^{-1}$, while Sh2-88 appears also in a region relatively free of neutral material at ≃+23 km s$^{-1}$.

## 4. Results

### 4.1. Radio continuum observations at 1420 and 408 MHz

The radio continuum images at 1420 and 408 MHz are shown in Fig. 1. The names of the HII regions as well as the positions of the O-type stars are given in Fig. 1a. Extended emission associated with Sh2-88 and Sh2-87 can be detected at both frequencies, along with some small diameter sources projected onto the HII regions. The compact HII regions Sh2-88A and Sh2-88B do not appear spatially resolved in our data. They can be identified as the strong sources at RA, Dec (J2000) = $19^h46.7^m$, $+25°10'$ in Fig. 1a. The extended source at RA, Dec (J2000) = $19^h44.3^m$, $+25°49'$ is identified with G61.7+0.9 (Altenhoff et al. 1970).

The image at 1420 MHz also reveals faint emission ($\Delta T \approx$ 0.3 K) covering an area of about $1.^\circ0 \times 0.^\circ8$ including the HII regions. Weak emission is also apparent in the image at 408 MHz. At this frequency, Sh2-88AB appears connected with sources near RA, Dec (J2000) = $19^h47.7^m$, $+24°50'$. It is not clear whether the HII regions in this area are physically related to each other.

### 4.2. Infrared emission

Figure 2 displays an overlay of the infrared emission at 60 $\mu$m, which enables us to investigate the dust distribution, and the radio continuum emission at 1420 MHz.

Sh2-88A, Sh2-88B and Sh2-87 are easily identified at IR wavelengths. Extended IR emission coincides with the radio continuum emission at 1420 MHz corresponding to Sh2-87, while the brightest infrared emission arises from Sh2-87 itself. Sh2-88 appears projected onto a faint *plateau* of emission which extends over part of the image. G61.7+0.9 coincides with weak extended emission, the brightest radio emission region correlating with an IRAS point source (Reich et al. 1986). Based on the present infrared data, it is not clear whether the weak *plateau* is associated with Sh2-88. The images at 12, 25 and 100 $\mu$m, which are not shown here, are similar to that at 60 $\mu$m.

### 4.3. HI line observations

In order to facilitate the display of the images, a constant background, equal to the mean value of each channel map within an area of $50'$ in radius centered at the field center, was subtracted from every line map. Figure 3 (*top panel*) displays the subtracted profile, which corresponds to the single dish average spectrum within that area. This profile illustrates the general characteristics of the HI emission in the direction of the Of stars. The bottom panel shows the kinematic distances toward $l = 61°$ as obtained from Brand & Blitz (1993) (assuming $R_0$ = 8.5 kpc and $\Theta_0$ = 220 km s$^{-1}$) using an analytical fit to the galactic rotation curve.

The average profile indicates the presence of significant emission within the velocity interval –100 to +50 km s$^{-1}$. According to circular galactic rotation models, HI at negative velocities should be located at kinematic distances $d_k \geq$ 10 kpc. Material with velocities $v \simeq 0$ km s$^{-1}$ is probably associated with the local arm and the Perseus arm at $d_k$ = 8–9 kpc (Georgelin & Georgelin 1976). HI at positive velocities is likely to be related to the local arm (Cohen et al. 1980).

The bottom panel of Fig. 3 also illustrates the large uncertainties in estimating kinematic distance along the line of sight to $l = 61°$, due to both the distance ambiguity and mainly to the small velocity gradient for distances below 8 kpc.

For distances in the range 2–3 kpc, compatible with the distance to both the Of stars and the HII regions (see Sect. 2), the galactic rotation curve predicts velocities of ≃22–29 km s$^{-1}$. A similar velocity is expected taking into account the observed velocity pattern for this section of the galaxy displayed in Fig. 2b of Brand & Blitz (1993). Consequently, in searching for cavities and holes that may be associated with the Of stars, we will pay particular attention to positive velocities.

For completness, we show in Fig. 4 the HI emission within the velocity interval –37.3 to +52.4 km s$^{-1}$ at intervals of 9.9 km s$^{-1}$. Each image is the average of six consecutive line maps. The images at different velocity intervals reveal HI emission covering most of the surveyed field and a number of holes and shells of a variety of sizes. Small scale structure is also present within the cavities and shells.

BD +24°3866 and BD +24°3881 are seen projected onto the inner part or the borders of some cavities. An HI cavity is present in the line of sight to BD +24°3866 in the image corresponding to 22.0 to 31.9 km s$^{-1}$ (Fig. 4). This feature is delineated by the larger ellipse in the image spanning that velocity range. This star also appears projected onto the borders of large holes in the images spanning the ranges (–37.3, –27.4) km s$^{-1}$, (–17.6, –7.7) km s$^{-1}$ and (+12.1, +22.0) km s$^{-1}$. BD +24°3881 appears projected onto an HI cavity in the image displaying material in the interval (+2.2, +12.1) km s$^{-1}$. Finally, both BD +24°3866 and BD +24°3881 are seen in projection onto

**Table 2.** O-type stars belonging to Vul OB1 within the field.

| Name | Sp.T. | RA (J2000) | Dec (J2000) | $\mu_{\rm RA}\cos\delta$ | $\mu_{\rm Dec}$ | $RV_{\rm LSR}$ |
|---|---|---|---|---|---|---|
| | | h m s | ° ′ ″ | mas/yr | mas/yr | km s$^{-1}$ |
| BD +24°3866 | O8.5II(f) | 19 45 40.6 | 25 07 36.1 | –1.0 ± 1.6 | –1.6 ± 1.6 | 9.4 ± 1.7 |
| BD +25°3952 | O8 | 19 45 42.1 | 25 21 16.4 | –4.2 ± 1.8 | –2.2 ± 1.8 | 18.6 ± 3.1 |
| BD +24°3881 | O6.5III(f) | 19 47 02.7 | 24 50 55.6 | –4.4 ± 1.2 | –1.1 ± 1.1 | |

a low HI emission region in the image showing the emission between +41.8 and +52.4 km s$^{-1}$. As we show below, these features are unrelated to the massive stars.

Based on the galactic rotation curve and previous molecular and optical observations of the ISM at about 2.4 kpc (see Sect. 2), we expect the signatures of the interaction between the Of stars and their local ISM to be detected at velocities of about +25 km s$^{-1}$. These considerations strongly favor the HI feature detected in the velocity range 22.0 to 31.9 km s$^{-1}$ as being related to BD +24°3866. Galactic rotation models predict kinematic distances $d_{\rm k}$ >9 kpc for the features at –32 and –12 km s$^{-1}$, while velocities >35 km s$^{-1}$ are forbiden for this section of the Galaxy. Thus, the structures at these velocities are most probably unconnected with the O-type stars.

To investigate the effects of the Of stars on the surrounding gas in more detail and the possible existence of neutral gas interacting with the HII regions, we will focus on the HI emission in the velocity range from +10 to +35 km s$^{-1}$ using the full velocity resolution images.

Figure 5 shows a series of images at constant velocity in steps of 1.65 km s$^{-1}$. For the sake of clarity, some of the radio continuum contours at 1420 MHz along with the position of the O stars are indicated in the images. As pointed out by Ehlerová et al. (2001), the neutral gas distribution within the velocity interval +10 to +30 km s$^{-1}$ is quite complex, revealing a lot of small scale structure with cavities and envelopes of varying shapes and sizes.

A strong absorption feature is detected at the position of Sh2-88A and Sh2-88B (RA, Dec (J2000) = $19^{\rm h}46.8^{\rm m}$, +25°10′.6), within the velocity range (+1.4, +25.0), suggesting that the neutral gas spanning this velocity interval should be at distances ≤ 2.5 kpc. It can be identified as the white spot coincident with the HII regions.

#### 4.3.1. HI related to BD +24°3866

Inspection of the HI emission at +24.5, +26.2, +27.8 and +29.5 km s$^{-1}$ (Fig. 5) discloses a region of low emission centered at RA, Dec (J2000) = $19^{\rm h}45.5^{\rm m}$, +25°15′.9 that is surrounded by an almost complete envelope. The later is clearly seen toward the north, east, and south of BD +24°3866 as a bright arc extending from RA, Dec (J2000) = $19^{\rm h}46^{\rm m}$, +25°30′.0 to $19^{\rm h}45.5^{\rm m}$, +24°50′.0. Toward the west, a patchy envelope is observed near RA, Dec (J2000) = $19^{\rm h}44^{\rm m}$, +25°15′.0. The Of star BD +24°3866 appears projected closer to the southern border of the HI minimum. This feature can also be seen in channel maps at both lower (down to +22.9 km s$^{-1}$) and higher (up to +31.1 km s$^{-1}$) radial velocities. From here on, this feature will be called Structure A. This feature is delineated by an ellipse in the image at 27.8 km s$^{-1}$.

The top panel of Fig. 6 displays the average HI brightness temperature distribution for this structure within the velocity interval +23.7 to +30.3 km s$^{-1}$. Structure A, indicated by an ellipse, is about 1.1° × 0.7° in size. It is also delineated in the bottom panel of the same figure after subtracting the large scale structures from the top panel following the procedure by Cichowolski et al. (2001).

As pointed out before, the systemic velocity of the structure ($v_{\rm sys} \simeq$ +27 km s$^{-1}$) is compatible with the published distance to Vul OB1 and BD +24°3866. Thus, the location of the star within the borders of the cavity suggests that Structure A may be related to the star.

Additional support for this association comes from the proper motion information. The arrow in the bottom panel of Fig. 6 indicates the direction of the tangential motion of the star and its uncertainty taking into account the quoted errors (see Table 2). At the adopted distance of 2.4 kpc, the tangential motion of the star is ≃22 ± 19 km s$^{-1}$. From the direction of the proper motion, the eccentric location of the star can be explained by the motion of the star toward the SE. Thus, a genetic relationship between the star and the HI feature can be established.

The HI bubble related to this star is slightly elongated. Weaver et al. (1977) showed that an interstellar bubble linked to a star with a relatively high spatial velocity becomes distorted in the direction of the stellar motion. We note, however, that the stellar velocity of BD +24°3866 is relatively low and does not seem to have distorted the bubble. The elongated shape of this bubble, in the SE-NW direction, could be explained by an asymmetric stellar wind, the non-uniform local insterstellar medium or the action of the local interstellar magnetic field.

As mentioned before, a number of HI cavities are detected in the line of sight to BD +24°3866 at different velocities (see Sect. 4.3). However, based on their kinematic distances, they are most probably unconnected with the Of star and are not considered further in this paper.

#### 4.3.2. HI associated with Sh2-88 and Sh2-87

The comparison between the radio continuum emission of Sh2-88 and the HI brightness temperature distribution (Fig. 5) reveals that this HII region is seen projected onto the innermost part of Structure A. Sh2-88 is closely surrounded by a chain of cloudlets detectable along the range +21.2 to +24.5 km s$^{-1}$ northwards and eastwards of the HII region.

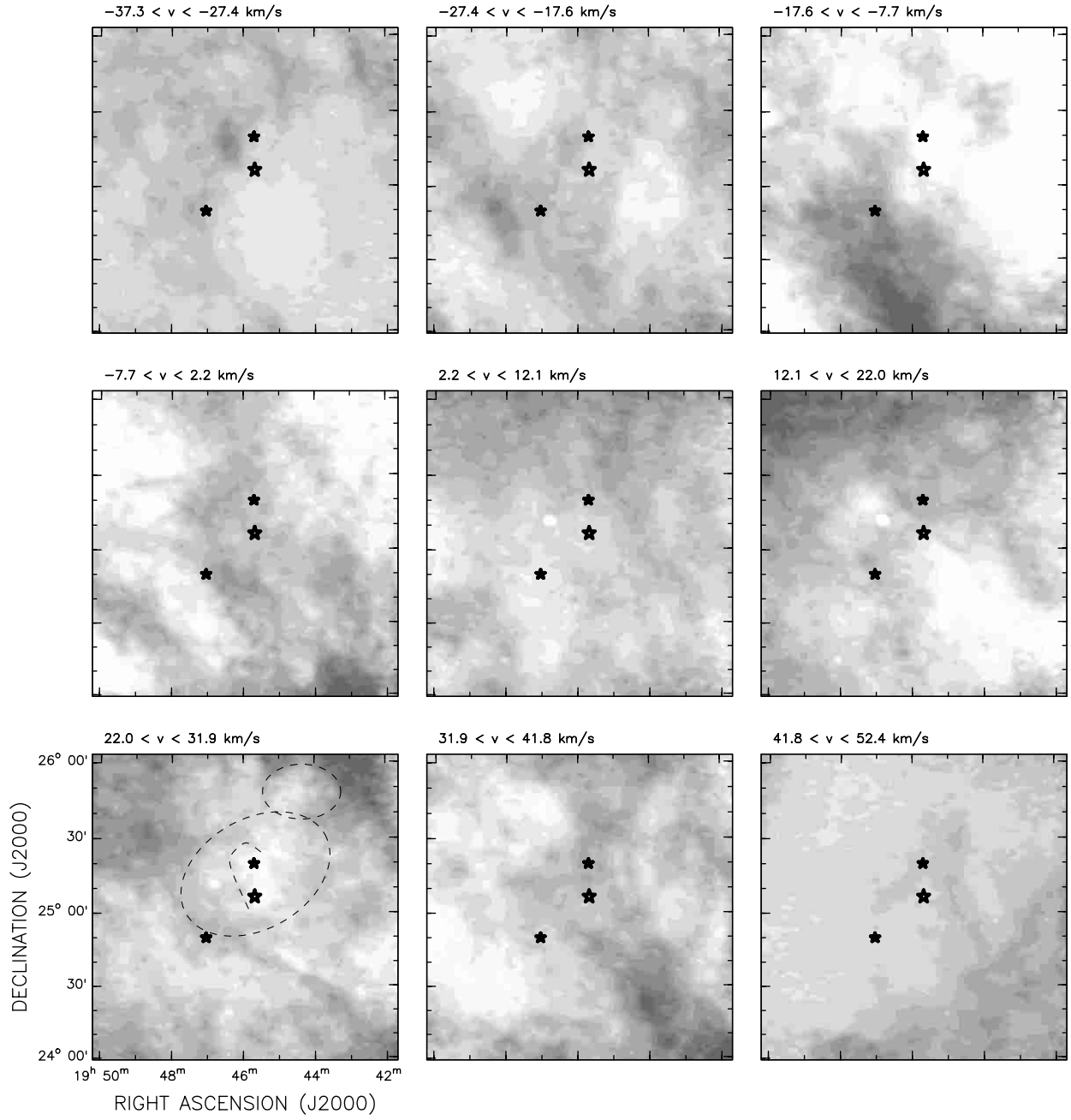


**Fig. 4.** Gray scale images showing the HI within the velocity range –37.3 to +52.4 km $s^{-1}$ in steps of 9.9 km $s^{-1}$. The velocity interval is indicated in the upper left corner of each image. The large star marks the position of BD +24°3866, while the small filled in stars indicate the position of the other two O-type stars in the area. The gray scale corresponds to –15 to 30 K in steps of 5 K. The ellipses in the image spanning the range 22.0 to 31.9 km $s^{-1}$ delineate HI features associated with BD +24°3866, Sh2-88 and G61.7+0.9 (see Sects. 4.3.1, 4.3.2 and 4.3.3).

This feature will be named Structure B and is delineated in the image spanning the range 22.0 to 31.9 km $s^{-1}$ in Fig. 4 and in the map at 22.9 km $s^{-1}$ in Fig. 5.

Figure 7 displays the radio continuum emission at 1420 MHz (*contour lines*) superposed onto Structure B (*grayscale*). The remarkable anticorrelation between neutral and ionized gas is clearly seen in the figure.

The agreement between the systemic velocity of Structure B ($\simeq$23 km $s^{-1}$) and the velocity of the H$\alpha$ and molecular lines in Sh2-88 (see Sect. 2), along with the morphological anticorrelation between the HI structure and the HII region strongly suggest that the HII region is interacting with the neutral gas.

The signature of the interaction of Sh2-88A and Sh2-88B with the surrounding gas should be observed at velocities $\simeq$+22 km $s^{-1}$ (see Sect. 3). However, from the present data, it is difficult to draw firm evidence in favor of such interaction because of the small size of the HII regions and the presence of strong absorption in the HI maps at positive velocities up to $\simeq$+25.0 km $s^{-1}$ (see Fig. 5). As mentioned in Sect. 4.3, the absorption in the HI line emission is seen as the white spot coincident with Sh2-88A and Sh2-88B.

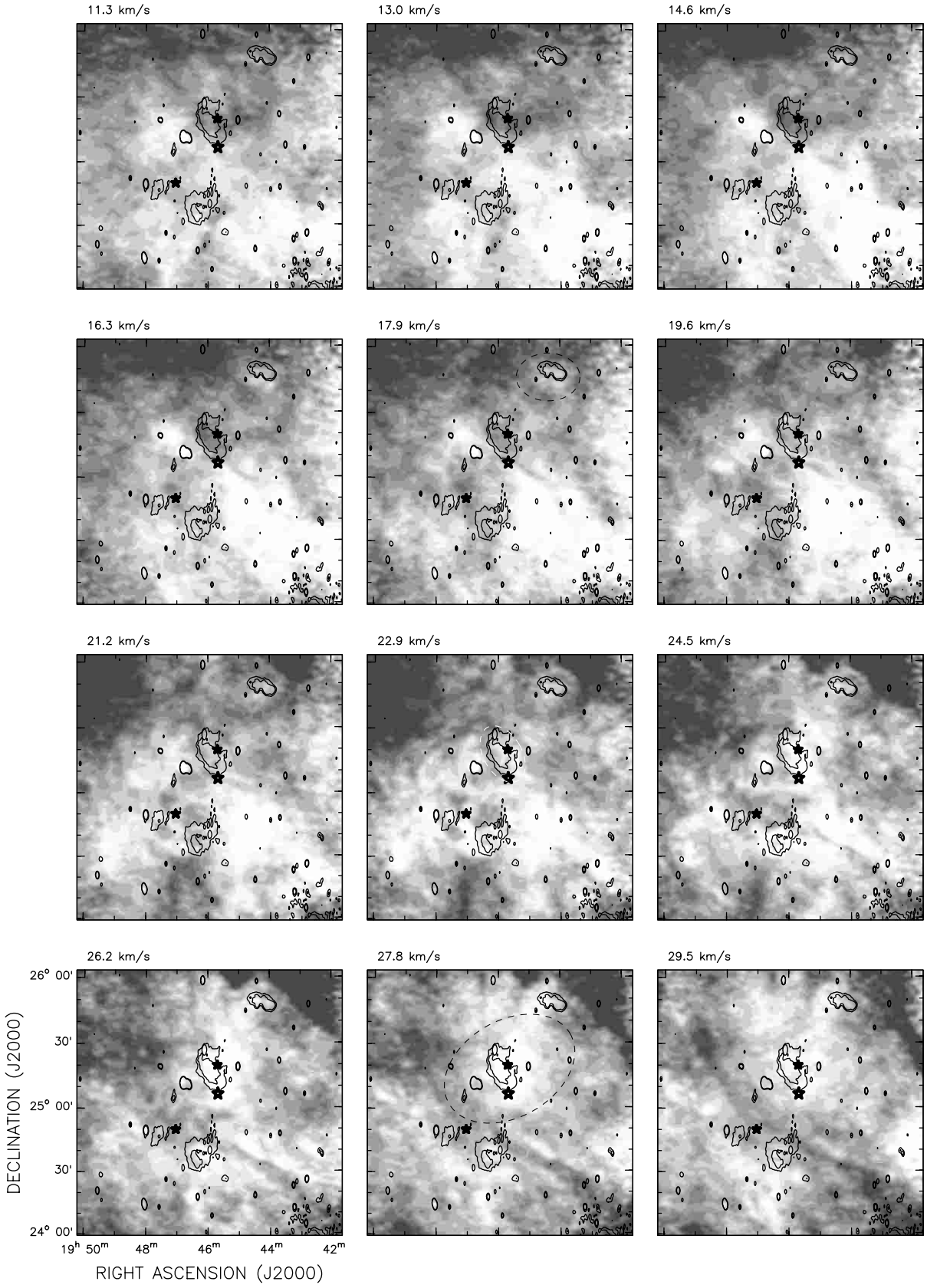


**Fig. 5.** Overlay of 1420 MHz contour lines and gray scale images showing the HI emission distribution within the velocity range 11.3 to 34.4 km $s^{-1}$ in steps of 1.65 km $s^{-1}$. The central velocity of each image is indicated in its upper left corner. The large star marks the position of BD +24°3866, while the small stars indicate the position of the other two O-type stars. The ellipses in the images at 17.9, 22.9 and 27.8 km $s^{-1}$ show the features related to G61.7+0.9, Sh2-88 and BD +24°3866. The gray scale corresponds to –15 to 25 K in steps of 5 K. Contour levels are 9.0 and 10.0 K.

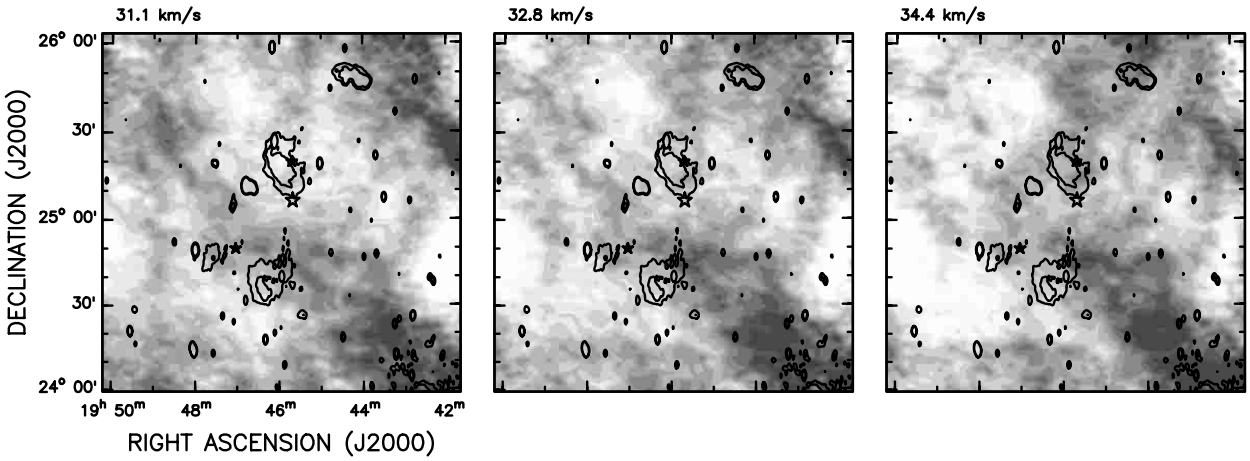


**Fig. 5.** continued.

The HII region Sh2-87 appears encircled by weak HI emission in the images at 26.2 and 27.8 km s$^{-1}$ in agreement with previous findings (Ehlerová et al. 2000). However, the present HI data do not enable us to firmly identify neutral gas associated with the HII region.

#### 4.3.3. HI associated with G61.7+0.9

HI probably linked to G61.7+0.9 can also be distinguished in the images corresponding to the velocity range 11.3 to 31.1 km s$^{-1}$, where an HI cavity and an envelope are clearly seen. This feature will be named Structure C. It is displayed in Fig. 8 and is delineated with the small ellipse in Figs. 4 and 5 (see the image at 17.9 km s$^{-1}$ in this last figure). The cavity coincides with the radio emission at 21 cm, increasing its size toward greater velocities, until it reaches a diameter of about 30′. The angular separation between Structures B and C is evident in the lower panel of Fig. 6. We note that for $v > 23$ km s$^{-1}$, the hole merges with Structure B.

Adopting $V_{\rm sys} \simeq 20$ km s$^{-1}$, the kinematic distance of Structure C is ≃2.0 or ≃6.5 kpc (near and far kinematic distances according to the bottom panel of Fig. 3) or in the range 1.2–3 kpc (based on the observed velocity pattern for this section of the galaxy displayed in Fig. 2b by Brand & Blitz 1993). Consequently, we adopted a distance $d = 2.4$ kpc for Structure C, in agreement with the distances of the other objects.

#### 4.3.4. The ISM around BD +24°3881

BD +24°3881 appears projected onto the SE border of a small HI low emission region in the image at 22.9 km s$^{-1}$ (Fig. 5) and onto an elongated HI cavity within the velocity interval 2.2 to 12.1 km s$^{-1}$ (Fig. 4).

The former feature, of ≈6.′6 in diameter (≃5 pc), is observed within a narrow velocity range. The direction of the proper motion of the star (toward the SW, see Table 2) cast doubts on the actual association between BD +24°3881 and the HI feature. The narrow velocity range also favors an interpretation as small scale density inhomogeneities in the general ISM.

Regarding the second structure, two facts cast doubts on its association with BD +24°3881. On the one hand, the kinematic distance derived for this feature is ≃0.5 kpc, quite different from the estimated spectrophotometric stellar distance. On the other hand, the direction of the stellar proper motion would indicate that BD +24°3881 is moving toward the center of the cavity, thus making a genetic relation between the star and the cavity unlikely. These facts preclude this feature as being related to the star.

The lack of a detectable feature associated with BD +24°3881 could be explained if the ambient gas density in the environs of the star were high. Confusion effects due to the presence of foreground and background neutral gas with velocities ≈25 km s$^{-1}$ might also mask an HI cavity related to this star.

## 5. Discussion

### 5.1. The ionized gas

Tables 3 and 4 summarize the main parameters of the bright small diameter sources and the HII regions. Spectral indices $\alpha$ are defined as $S_\nu \propto \nu^\alpha$.

There are a number of small diameter sources projected near Sh2-87, Sh2-88 and G61.7+0.9 and onto the faint *plateau*. Their coordinates, along with their flux densities at 327 and 1420 MHz and spectral indices are listed in Table 3. The sources are shown in Fig. 9. Flux densities at 327 MHz were obtained from the compact source catalog (Taylor et al. 1996). These observations have a synthesized beam of about 1.′0 × 2.′4 in this section of the Galaxy. Flux densities listed in the NVSS catalog (Condon et al. 1998) are also included. Flux densities at 408 MHz have large error because of background emission and calibration uncertainties and are not included in the table. The derived spectral indices indicate that sources 2, 6 and 7 are likely to be thermal, while the rest of the sources are non-thermal and probably extragalactic in origin. Taylor et al. (1996) found similar spectral indices for sources 6 and 7. Source 2 is optically thick at 408 MHz as found by Reich et al. (1986). It coincides with an IR point source (see Fig. 2 and Sect. 2). Source 6 is the UC region Sh2-87 and is projected

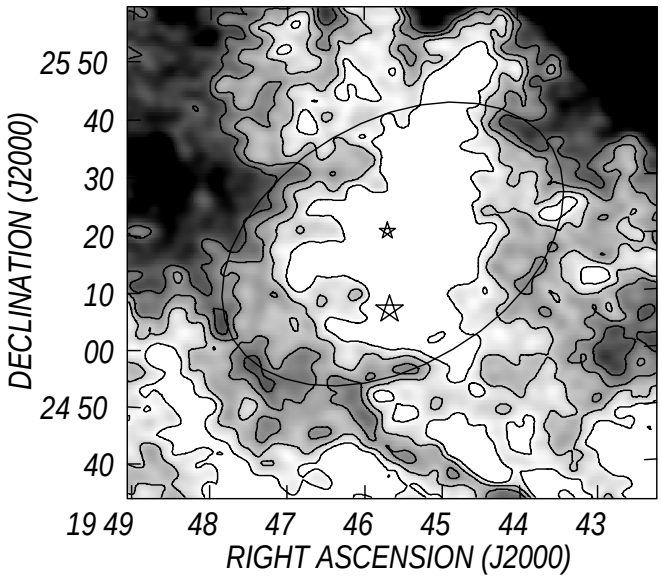


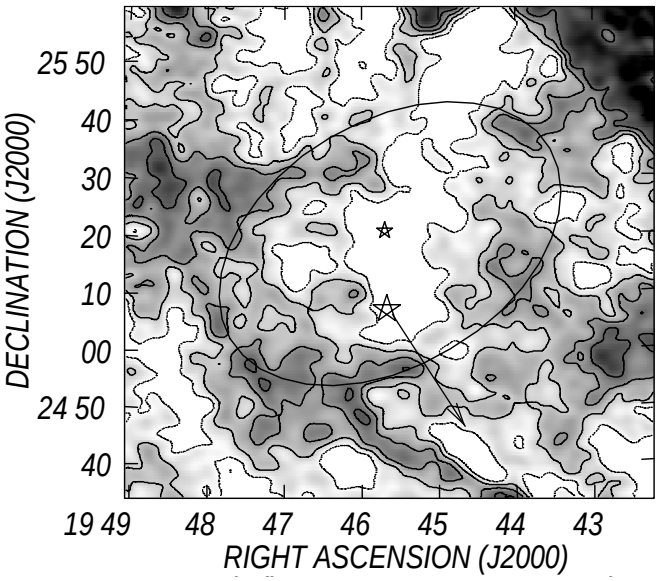


**Fig. 6.** *Top panel.* Average HI brightness temperature distribution for Structure A within the velocity range 23.7 to 30.3 km $s^{-1}$. The star symbols indicate the position of BD +24°3866 and BD +25°3952. The gray scale is 75 to 100 K. Contour levels are 75 to 90 K in steps of 5 K. *Bottom panel.* Same as top panel after subtracting the large scale structures. The gray scale is –5 to 20 K. Contour levels are –5 to 10 K in steps of 5 K.

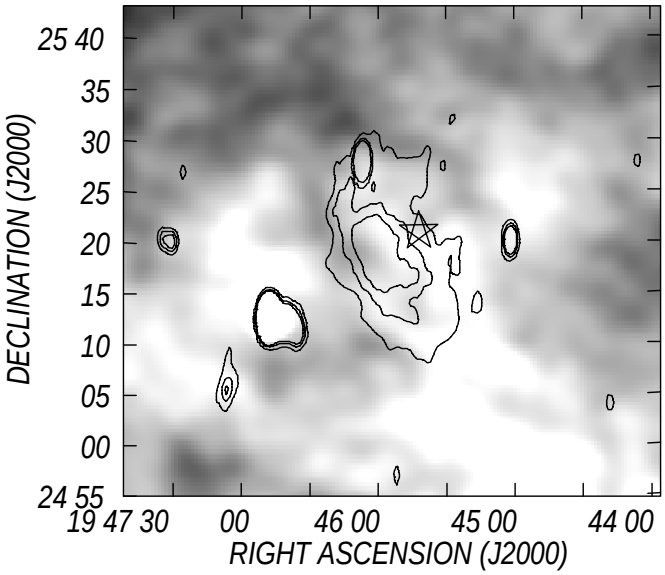


**Fig. 7.** Overlay of the HI column density distribution for Structure B *(grayscale)* and the radio continuum emission at 1420 MHz for Sh2-88. The HI image corresponds to the velocity range 18.8 to 25.3 km $s^{-1}$. The star symbol indicates the position of BD +25°3952. The gray scale is (9.5–14.0) × $10^{20}$ $cm^{-2}$. Contour levels are 9.0, 10.0 and 11.0 K.

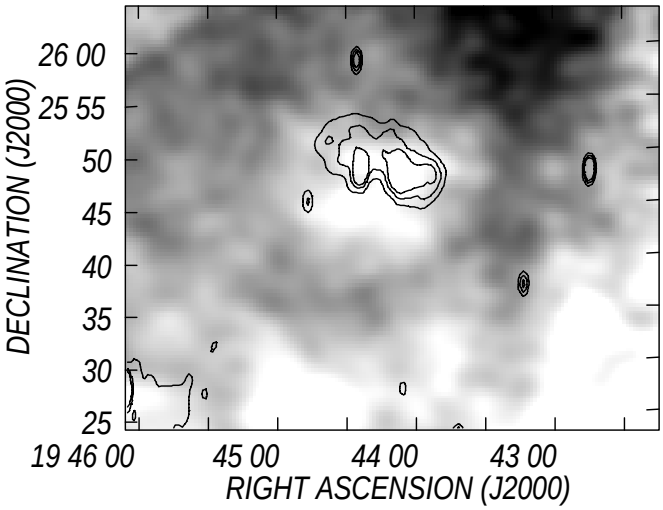


**Fig. 8.** Overlay of the HI column density image for Structure C (*grayscale*) and the radio continuum emission of G61.7+0.9 *(contour lines)*. The HI image was obtained through the velocity range 15.5 to 23.7 km $s^{-1}$. The gray scale is (13.5–18.0) × $10^{20}$ $cm^{-2}$. Contour levels are 9.0, 10.0 and 11.0 K.

onto diffuse extended emission probably related to this HII region. Sh2-88A and Sh2-88B are detected as two strong unresolved sources. They are definite thermal sources and are not listed in the table. The contribution from non-thermal sources was subtracted from the quoted flux densities of the HII regions.

Emission measure $EM$, electron density $n_e$ and ionized mass $M_i$ for the HII regions were obtained using the expressions by Mezger & Henderson (1967) based on the measured flux densities at 1420 MHz and the sizes listed in Table 4. The adopted electron temperatures and volume filling factors were $T_e = 10^4$ K and $f = 1$, respectively. For the case of Sh2-87, we have discriminated between the compact and the extended regions. The derived ionized mass was multiplied by 1.27 to take into account singly ionized He (see Goss & Lozinskaya 1995). The distance to Sh2-87 and G61.9+0.9 is 2.4 kpc.

Based on Effelsberg data, Reich et al. (1986) found a 1420 MHz flux density $S_\nu = 1.9 \pm 0.2$ Jy for G61.7+0.7. This value is larger than our estimate and is likely due to the presence of radio continuum emission unconnected to this source (Effelsberg beam at 1420 MHz is 9′). The UV photon flux

**Table 3.** Small diameter radio sources.

| # | RA(J2000) (h m s) | Dec(J2000) (° ′ ″) | $S_{327}$ (mJy) | $S_{1420}$ (mJy) | $S_{\rm NVSS}$ (mJy) | $\alpha$ | Comm. |
|---|---|---|---|---|---|---|---|
| 1 | 19 44 06.7 | 25 48 39 | 218 ± 16 | 113 ± 7 | 43.4 ± 2.0 | –0.8 ± 0.3 | onto G61.7+0.9 |
| 2 | 19 44 23.6 | 25 48 52 | 69 ± 6 | 85 ± 5 | 78.2 ± 2.6 | +0.11 ± 0.03 | onto G61.7+0.9 |
| 3 | 19 45 01.7 | 25 20 17 | 363 ± 4 | 101 ± 2 | 92.0 ± 2.8 | –1.0 ± 0.1 | near Sh2-88 |
| 4 | 19 45 56.4 | 24 41 14 | 212 ± 7 | 78 ± 3 | 75.6 ± 2.3 | –0.68 ± 0.03 | near Sh2-87 |
| 5 | 19 46 06.9 | 25 28 10 | 695 ± 6 | 263 ± 3 | 264.7 ± 9.3 | –0.8 ± 0.2 | near Sh2-88 |
| 6 | 19 46 21.0 | 24 35 13 | 358 ± 7 | 563 ± 3 | 545.3 ± 20.4 | +0.30 ± 0.02 | Sh2-87 (UC) |
| 7 | 19 48 00.2 | 24 50 19 | 220 ± 5 | 242 ± 5 | 219.9 ± 8.3 | +0.03 ± 0. | |

**Table 4.** HII regions: radio characteristics.

| HII region | $S_{1420}$ (Jy) | Size (′ × ′) | Size pc | $EM$ ($10^2$ pc cm$^{-6}$) | $n_{\rm e}$ (cm$^{-3}$) | $M_{\rm i}$ ($M_\odot$) |
|---|---|---|---|---|---|---|
| Sh2-88 | 2.01 | 21 × 9 | 14.7 × 6.3 | 11.4 | 9 | 410 |
| Sh2-87 (UC) | 0.56 | 2 × 0.9 | 1.4 × 0.6 | 335 | 160 | 6.6 |
| Sh2-87 (extended) | 0.66 | 10 × 9 | 7.0 × 6.3 | 7.8 | 9 | 135 |
| G61.7+0.9 | 1.06 | 11 × 6 | 7.7 × 4.2 | 17.2 | 15 | 135 |

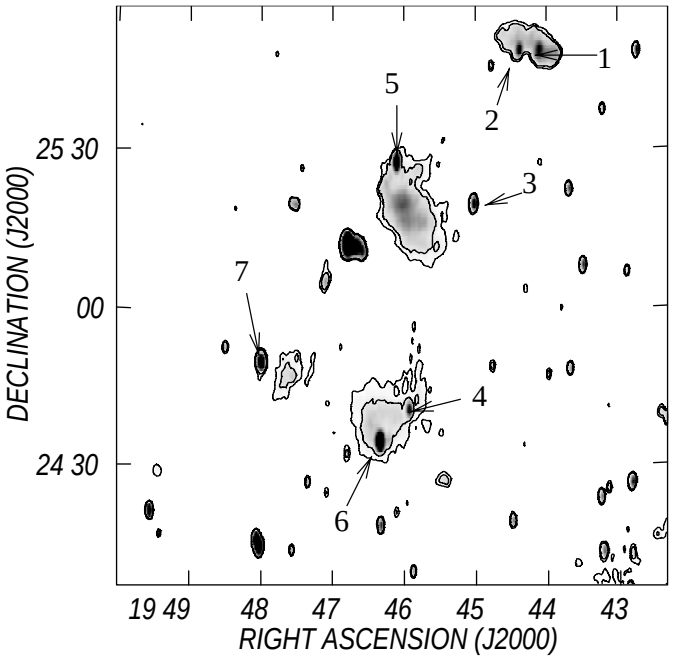


**Fig. 9.** Radio continuum image at 1420 MHz showing the position of the small diameter sources listed in Table 3.

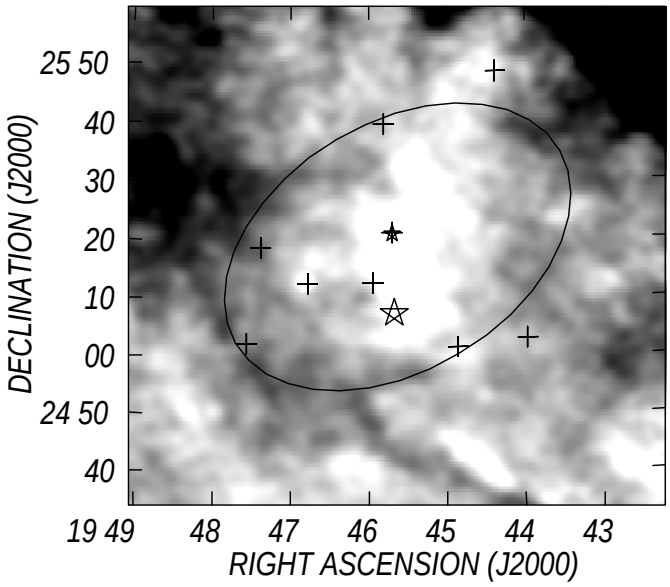


**Fig. 10.** As Fig. 6a but showing the position of the IRAS point like sources projected onto the HII regions and Structure A. The grey scale corresponds to 70 to 100 K.

needed to keep the HII region ionized is, according to our results, $N_{\rm L} \simeq 2{\times}10^{47}$ s$^{-1}$ which can be provided by a B0.5V star (Vacca et al. 1996).

### 5.2. The heated dust

Table 5 summarizes the flux density estimates at 60 and 100 $\mu$m obtained for the HII regions present in the area. For Sh2-87 we have discriminated between the extended and the UC HII region. Based on the derived flux densities and standard dust grain parameters (e.g. Draine & Lee 1984), rough estimates of the dust temperature and mass were obtained (see Cichowolski et al. 2001). Dust temperatures are indicated for $n$ = 1.5–2. This parameter is related to the dust absorption efficiency $\kappa_\nu \propto \nu^n$, normalized to 40 cm$^2$ g$^{-1}$ at 100 $\mu$m. The derived dust temperatures are typical for HII regions (e.g. Fich & Terebey 1996).

### 5.3. Main parameters of the structures

It is clear from Sect. 4 that the whole HI emission distribution reveals neutral material related to different astronomical objects in the same line of sight and within similar velocity intervals.

The main parameters of structures A, B and C are summarized in Table 6. The velocity interval $v_1, v_2$ corresponds to the interval where the HI structures can be identified. The systemic velocities $v_{sys}$ indicate the velocity where the features present their deepest temperature gradient and largest dimensions. Kinematic distances for the three structures are in the range 2–3 kpc, in agreement with photometric distances to BD +24°3866, Vul OB1, Sh2-88 and Sh2-87. The semimajor and semiminor axes of the structures ($r_M \times r_m$) are defined by the position of the maxima in the shells. The equivalent radius $R_S$ was obtained as the harmonic mean of the two axes. The neutral mass in the shells $M_n$ was evaluated assuming the optically thin case and a typical interstellar He abundance of 10%. For Structure A, the associated neutral mass was estimated from the bottom panel of Fig. 6.

The ambient density $n_o$ was evaluated by uniformly distributing the neutral mass $M_n$ and the associated ionized mass $M_i$ over the volume of the structure. Ionized masses were derived in Sect. 5.1. Although some molecular emission detected in the environs of Sh2-88 by Helfer & Blitz (1997) (see their Fig. 2) is probably associated with Structure B, its molecular mass is difficult to estimate.

A lower limit to the expansion velocity of the structures can be estimated as $V_{exp} = (v_2 - v_1)/2 + 2.4$ km s$^{-1}$. Here $v_1$ and $v_2$ are the lowest and highest velocities at which the structures are observed. The extra 2.4 km s$^{-1}$ allows for the possible presence of HI in the *caps* of the expanding shell. For Structures A and B, $V_{exp} \approx 7$ km s$^{-1}$, while it is ≈13 km s$^{-1}$ for Structure C. As a working hypothesis we adopted a mean expansion velocity of $10 \pm 3$ km s$^{-1}$. We estimate the kinetic energy $E_k$ of all structures taking into account the neutral and the ionized masses.

The major source of error in radii, masses and kinetic energies is the distance uncertainty. An error of 25% in the distance implies a 25% error in radius and 50% error in the derived masses. The uncertainty in the kinetic energy is at least 80% assuming a 30% error in the expansion velocity. Uncertainty in the derived ambient density is about 100%.

### 5.4. The origin of the structures

In this section we investigate the relation between the HI structures and the optical objects. As a working hypothesis, we assume that Structure A is an expanding feature related to BD +24°3866. The systemic velocity of Structure B is slightly smaller than the corresponding one for Structure A. This fact, along with the projection of Structure B onto the central region of Structure A suggests that Structure B and Sh2-88 are located in the approaching part of Structure A. In this case both BD +24°3866 and BD +25°3952 (the exciting star of Sh2-88) would be powering both structures. The difference in the ambient density $n_o$ derived for Structures A and B also supports the idea that Structure B is evolving in the envelope of Structure A.

It is well known that massive stars possess strong stellar winds which create relatively large cavities and shells in the ISM. To test whether BD +24°3866 and BD +25°3952 can provide the energy to power Structures A and B, we have estimated the mechanical energy $E_w$ released into the ISM during the dynamical age $t_d$ of the structure and compared it to the kinetic energy $E_k$ of Structures A and B as a whole.

For an interstellar bubble, the dynamical age can be evaluated as $t_d = 0.55 \times 10^6\ R_S/V_{exp}$ yr (McCray 1983), where $R_S$ is the equivalent radius of the bubble (pc), $V_{exp}$ is the expansion velocity (km s$^{-1}$) and the constant represents a mean value between the energy and the momentum conserving cases. Adopting the radius and expansion velocity of structure A, we find $t_d = 1.0 \times 10^6$ yr. With an initial mass of 30–50 $M_\odot$ for BD +24°3866 (Leitherer 1988), the estimated dynamical age is lower than the time needed by the star to evolve to its current phase ((3.5–6)×10$^6$ yr, Massey 1997; Meynet et al. 1994). The uncertainty in the dynamical age is about 50%. With a tangential velocity of ≃20 km s$^{-1}$ (see Sect. 4.3.1), the time taken by the star to cross the bubble is 2×10$^6$ yr. Consequently, we can adopt $t_d = 1.5\times10^6$ yr as a mean value. The derived dynamical age indicates that the stellar winds from both the main sequence phase of BD +24°3866 and its present evolutionary phase contributed in shaping the HI bubble.

To evaluate $E_w (= L_w t_d = \dot{M} V_w^2 t_d/2)$ we assume that only BD +24°3866 contributed to the formation of the bubble. We adopt a terminal velocity $V_w = 1500$ km s$^{-1}$ and a mass loss rate $\dot{M} = 1\times10^{-6}\ M_\odot$ yr$^{-1}$ in agreement with mean values from Prinja et al. (1990) and with the expression by Lamers & Leitherer (1993), respectively. The adopted values are conservative estimates for O8V-O9V stars. Thus, $E_w = 3.4\times10^{49}$ erg s$^{-1}$, with an uncertainty of about 90% assuming uncertainties of 50% in the mass loss rate and 30% in the terminal velocities.

The ratio $\epsilon$ between the kinetic energy $E_k$ of Structures A and B as a whole and the mechanical energy provided by the massive star is $\epsilon \simeq 0.03$. The uncertainty in this value is large. Taking into account current evolutionary models of interstellar wind blown bubbles, this value indicates that BD +24°3866 alone is capable of blowing the observed structure via stellar winds.

The location of BD +25°3952, the exciting star of Sh2-88, close to the center of the cavity and the direction of its tangential motion indicates that this star have also contributed in shaping Structure A. In addition, the UV photon flux from BD +25°3952 (e.g. Vacca et al. 1996) suffices to keep the diffuse HII region ionized even if this star is placed close to the center of the HI bubble.

Bearing in mind the above results, an estimate of the gas-to-dust ratio follows. According to Tables 5 and 6, the gas-to-dust ratio for the case of Sh2-88 is in the range 65–280 (the total gas mass is the ionized mass from Table 4 plus the neutral mass of Structure B from Table 6). Within errors, the derived values are compatible with the gas-to-dust ratio of 100, typical for the ISM. In Sh2-87, the gas-to-dust ratio is particularly low (<20) (here we only see the ionized gas in both the UC and the extended regions – see Table 4). This indicates that a large amount of undetected or unidentified neutral and molecular material is associated with the HII region. On the other hand, the derived ratio in G61.7+0.9 is high, probably suggesting the presence of clumping (in this case, the gas mass is the ionized mass from Table 4 and the neutral mass of Structure C from Table 6).

**Table 5.** HII regions: flux densities at 60 and 100 $\mu$m and dust parameters.

| HII region | $S(60\,\mu\mathrm{m})$ (Jy) | $S(100\,\mu\mathrm{m})$ (Jy) | $T_\mathrm{d}(n=1.5)$ (K) | $T_\mathrm{d}(n=2.0)$ (K) | $M_\mathrm{d}$ $M_\odot$ |
|---|---|---|---|---|---|
| Sh2-88 | 750 | 1420 | 32 ± 6 | 29 ± 5 | 2.0–8.7 |
| Sh2-87(UC) | 4320 | 5960 | 37 ± 8 | 33 ± 6 | 5.2–22.7 |
| Sh2-87(extended) | 1910 | 2440 | 38 ± 9 | 34 ± 7 | 1.9–8.3 |
| G61.7+0.9 | 315 | 370 | 40 ± 9 | 36 ± 7 | 0.3–1.1 |

**Table 6.** Parameters of the HI structures.

| | Structure A | Structure B | Structure C |
|---|---|---|---|
| Center coordinates | | | |
| RA(J2000) | $19^\mathrm{h}45\overset{\mathrm{m}}{.}5$ | $19^\mathrm{h}45\overset{\mathrm{m}}{.}8$ | $19^\mathrm{h}44\overset{\mathrm{m}}{.}3$ |
| Dec(J2000) | +25°15′.9 | +25°20′.0 | +25°45′.0 |
| Vel. interval $v_1, v_2$ (km s$^{-1}$) | +21.6, +32.4 | +18.3, +29.1 | +10.0, +32.4 |
| Systemic vel. $v_\mathrm{sys}$ (km s$^{-1}$) | +27 | +22 | +20 |
| Adopted distance $d$ (kpc) | 2.4 | 2.4 | 2.4 |
| Semiaxes of the envelope (′) | 33 × 21 | 13 × 8 | 14 |
| Semiaxes of the envelope (pc) | 23 × 15 | 9 × 6 | 10 |
| Equivalent radius (pc) | 19 | 7.4 | 10 |
| $M_\mathrm{n}$ ($M_\odot$) | 760 | 150 | 200 |
| $M_\mathrm{i}$ ($M_\odot$) | – | 410 | 135 |
| $n_\circ$ (cm$^{-3}$) | 1 | 14 | 4 |
| $V_\mathrm{exp}$ (km s$^{-1}$) | 10 | 10 | 10 |
| $E_\mathrm{k}$ ($10^{48}$ erg) | 0.76 | 0.15 | 0.36 |
| Related object | BD +24°3866 | Sh2-88 | G61.7+0.9 |
| | BD +25°3952 | BD +25°3952 | |

Blitz (1980) lists stellar winds from massive stars as a mechanism to induce the collapse of interstellar clouds and trigger star formation. Since there are signs of star formation in the environs of the massive stars, this region seems ideal to investigate a possible relation between star formation and interstellar bubbles. According to Deharveng et al. (2000), the Sh2-88 region as a whole presents a case of sequential star formation. These authors have found that star formation seems to have progressed along a southwest to northeast direction, from the HII region Sh2-88A to Sh2-88B. To investigate the presence of young stellar objects associated with Structures A and B, we analyzed the distribution of infrared point sources whose spectra fit the selection criteria established by Junkes et al. (1992). These radiation criteria allow to discriminate protostellar candidates from cold IRAS point sources related to planetary nebulae, cirrus clumps and cool stars.

Infrared protostellar candidates are spread mainly over the central and southern regions of the surveyed field. Three candidates are concentrated close to the center of Structure A. Two of them are projected onto Sh2-88: one of these sources is identified with BD +25°3952 (IRAS 19436+2514), the other appears projected onto the HII/HI interface region in Feature B (IRAS 19438+2505). The source IRAS 19446+2505 is associated with Sh2-88B, where star formation is present, and IRAS 19423+2541 correlates with the position of G61.7+0.9. The IRAS candidates 19427+2454, 19418+2455, 19452+2511, 19454+2454 and 19437+2532 appear projected onto Structure A. The position of these nine infrared sources is indicated in Fig. 10. Further observational studies are necessary to analyze the presence of molecular material related to Structure A and the possibility of star formation triggered by the wind blown bubble shock.

## 6. Conclusions

Based on radio continuum data at 408 and 1420 MHz and neutral hydrogen observations obtained with the DRAO Synthesis Telescope (synthesized beams of 7′ and 1′.5 at 408 and 1420 MHz, respectively) and high resolution infrared data, we analyzed the interstellar medium in the environs of the massive stars BD +24°3866, BD +24°3881 and BD +25°3952. The diffuse HII regions Sh2-88 and G61.7+0.9, and the compact HII regions Sh2-88A, Sh2-88B and Sh2-87 are projected within the same area. The main findings of our study can be summarized as follows:

*1.* The neutral gas data show an HI bubble around the O8.5II(f) star BD +24°3866. The massive star is close to the inner border of the HI shell. The slowly expanding shell is 24×15 pc in radius and its dynamical age is $\approx 1.5\times10^6$ yr, lower than the main sequence lifetime of the massive star.

*2.* The diffuse HII region Sh2-88, excited by the O8 star BD +25°3952, appears surrounded by an almost complete

HI structure of about 9×6 pc in radius which consists of a chain of cloudlets. The neutral and ionized masses associated with Sh2-88 are about 150 $M_\odot$ and 410 $M_\odot$, respectively, while the dust mass is in the range 2.0–8.7 $M_\odot$. The rms electron density is 9 cm$^{-3}$.

*3.* Sh2-88 appears to be evolving in the approaching cap of the large HI bubble. Thus, the total neutral mass associated with the HI bubble is about 1400 $M_\odot$. We interpret the HI structure as the neutral gas signature of the interaction of the stellar winds of BD +24°3866 and BD +25°3952 with their surroundings. Both stars are located inside the bubble, provide the energy and momentum to drive the expansion and are responsible for heating the dust. The UV photon flux provided by BD +25°3952 alone is enough to keep Sh2-88 ionized.

*4.* Several infrared protostellar candidates were found projected onto the HI bubble related to the massive stars, suggesting that star formation may be taking place in the shell. However, further studies are necessary to investigate the possibility of star formation triggered by the wind blown bubble shock.

*5.* A small HI shell was also found to be associated with the HII region G61.7+0.9. The shell is expanding at about 13 km s$^{-1}$ and is about 10 pc in radius. The associated neutral and ionized masses are 220 and 150 $M_\odot$, respectively. A kinematic distance of ≃2.4 kpc can be derived from the neutral gas data.

*6.* We were unable to find a definite HI feature related to either Sh2-87 or to the O6.5III(f) star BD +24°3881.

*Acknowledgements.* C.E.C. is grateful for the kind assistance of the DRAO staff during her stay at the Observatory. We specially thank R. Khotes for his help in processing interferometric data. We acknowledge the referee, Dr. Margarita Rosado, for many suggestions that improved the presentation of this study. We also thank F. Bareilles for his help with the figures and M.-L. Chaix for her help with the latex version. The DRAO Synthesis Telescope is operated as a national facility by the National Research Council of Canada. The work of E.M.A., C.E.C. and S.C. was partially financed by the Consejo Nacional de Investigaciones Científicas y Técnicas (CONICET) of Argentina under project PIP 607/98 and by Fundación Antorchas, Argentina, through project 13622/10. The work of S.P. is financed through grants from the Natural Sciences and Engineering Research Council of Canada and the Fonds FCAR from Québec.

## References

Altenhoff, W. J., Downes, D., Goad, L., Maxwell, A., & Rinehart, R. 1970, A&AS, 1, 319
Barbier-Brossat, M., & Figon, P. 2000, A&AS, 142, 217
Barsony, M. 1989, ApJ, 345, 268
Blair, G. N., Peters, W. L., & Vanden Bout, P. A. 1975, ApJ, 200, L161
Blitz, L. 1980, in Giant Molecular Clouds in the Galaxy, ed. P. M. Solomon, M. G. Edmunds (Oxford: Pergamon Press), 211
Brand, J., & Blitz, L. 1993, A&A, 275, 67
Bronfman, L., Nyman, L. A., & May, J. 1996, A&AS, 115, 81
Cappa, C. E., Dubner, G., Rogers, C., & St-Louis, N. 1996, AJ, 112, 1104
Cappa, C. E., & Herbstmeier, U. 2000, AJ, 120, 1963
Chlebowski, T., & Garmany, C. D. 1991, ApJ, 368, 241
Chu, Y. H., Treffers, R. R., & Kwitter, K. B. 1983, ApJS, 53, 920
Churchwell, E., Walmsley, C. M., & Cesaroni, R. 1990, A&AS, 83, 119
Cichowolski, S., Pineault, S., Arnal, E. M., et al. 2001, AJ, 122
Condon, J. J., Cotton, W. D., Greisen, E. W., et al. 1998, AJ, 115, 1693
Cohen, R. S., Cong, H., Dame, T. M., & Thaddeus, P. 1980, ApJ, 239, L53
Deharveng, L., Nadeau, D., Zavagno, A., & Caplan, J. 2000, A&A, 360, 1107
Douglas, J. N., Bash, F. N., Bozyan, F. A., Torrence, G. W., & Wolfe, C. 1996, AJ, 111, 1945
Draine, B. T., & Lee, H. M. 1984, ApJ, 285, 89
Ehlerová, S., Palous, J., & Huchtmeier, W. K. 2001, A&A, 374, 682
Felli, M., & Harten, R. H. 1981, A&A, 100, 42
Fich, M., & Blitz, L. 1984, ApJ, 279, 125
Fich, M., Treffers, R. R., & Dahl, G. P. 1990, AJ, 99, 622
Fich, M., & Terebey, S. 1996, ApJ, 472, 624
Forbes, D. 1989, A&AS, 77, 439
Fürst, E., Reich, W., Reich, P., & Reif, K. 1990, A&AS, 85, 691
Garmany, C. D., & Vacca, W. D. 1991, PASP, 103, 347
Garmany, C. D., & Stencel, R. E. 1992, A&AS, 94, 211
Georgelin, Y. M. 1975, Ph.D. Thesis, University of Marseille
Georgelin, Y. M., Georgelin, Y. P., & Roux, S. 1973, A&A, 25, 337
Georgelin, Y. M., & Georgelin, Y. P. 1976, A&A, 49, 57
Goss, W. M., & Lozinskaya, T. 1995, ApJ, 439, 637
Haslam, C. G. T., Salter, C. J., Stoffel, H., & Wilson, W. E. 1982, A&AS, 47, 1
Helfer, T. T., & Blitz, L. 1997, ApJ, 478, 233
Hog, E., Fabricius, C., Makarov, V. V., et al. 2000, A&A, 355, L27
Junkes, N., Fürst, E., & Reich, W. 1992, A&A, 261, 289
Kallas, E., & Reich, W. 1980, A&AS, 42, 227
Koo, B.-C., & McKee, C. F. 1992, ApJ, 388, 93
Lamers, H. J. G. L. M., & Leitherer, C. 1993, ApJ, 412, 771
Landecker, T. L., Dewdney, P. E., Burgess, T. A., et al. 2000, A&AS, 145, 509
Leitherer, C. 1988, ApJ, 326, 356
Lortet-Zuckermann, M. C. 1974, A&A, 30, 67
Lozinskaya, T. A. 1982, Ap&SS, 87, 313
Marston, A. P., Chu, Y.-H., & García-Segura, G. 1994, ApJS, 93, 229
McCray, R. 1983, Highlights of Astron., 5, 567
Massey, P. 1997, in The Stellar Initial Mass Function, proceedings of the 38th Herstmonceux Conference, ed. G. Gilmore, I. Parry, & S. Ryan
Mezger, P. D., & Henderson, A. P. 1967, ApJ, 147, 471
Meynet, G., Maeder, A., Schaller, G., Schraerern, D., & Charbonnel, C. 1994, A&AS, 103, 97
Miranda, A. I., & Rosado, M. 1987, Rev. Mex. Astron. Astrofis., 14, 479
Pilkingston, J. D. H., & Scott, P. F. 1965, MRAS, 69, 183
Pirigov, L., Zinchenko, I., Lapinov, A., Myshenko, V., & Shul'Ga, V. 1995, A&AS, 109, 333
Prinja, R. K., Barlow, M. J., & Howarth, I. D. 1990, ApJ, 361, 607
Reich, W., Fürst, E., Reich, E., Sofue, Y., & Handa, T. 1986, A&A, 155, 185
Sharpless, S. 1959, ApJS, 4, 257
Taylor, A. R., Goss, W. M., Coleman, P. H., van Leeuwen, J., & Wallace, B. J. 1996, ApJS, 107, 239
Turner, B. E. 1970, Astrophys. Lett., 6, 99
Vacca, D., Garmany, C. D., & Shull, J. M. 1996, ApJ, 460, 914
Weaver, R., McCray, R., Castor, J., Shapiro, P., & Moore, R. 1977, ApJ, 218, 377
White, G. J., & Fridlung, C. V. M. 1992, A&A, 266, 452
Williams, D. R. W. 1973, A&AS, 8, 505